5.1 RADAR CHARACTERISTICS OF VIOLENT TORNADIC STORMS USING THE NSSL ALGORITHMS ACROSS SEPARATE GEOGRAPHIC REGIONS OF THE UNITED STATES

National Weather Service

Chris Broyles * Amarillo, TX | **Richard Wynne** Amarillo, TX | **Neal Dipasquale** Sterling, VA | **Hector Guerrero** San Angelo, TX | **Tim Hendricks** San Angelo, TX

1. INTRODUCTION

Much work has been done in recent years concerning the National Severe Storms Laboratory (NSSL) algorithms relating to tornadic storms. Greg Stumpf (June 1998 Wea. Forecasting) recently lead the Tornado Warning Guidance project at NSSL to improve tornado warnings by associating tornado detections of the NSSL algorithms to ground truth. In addition, Carpenter et al. (2000) looked at the NSSL algorithms with respect to tornadoes in the Jackson, Mississippi National Weather Service county warning area. Also, Burgess and Magsig (1993, 1998 and 2000) identified various radar characteristics associated with the Red Rock, Oklahoma; Tulsa, Oklahoma; Louisville, Kentucky; Jarrell, Texas; and Oklahoma City, Oklahoma violent tornadoes. The purpose of this research is to expand on the work of previous studies by increasing the understanding of radar characteristics associated with violent tornadic storms and to determine the similarities and differences of the characteristics across separate geographic regions of the United States. For this study, 38 United States violent tornadic storms were analyzed from 1993 to 2001 using the NSSL algorithms. Storm types and environment characteristics were identified. In addition, radar signatures were recorded along with cell and meso parameters. As a result, radar characteristics favorable for violent tornadoes are presented for different geographic regions of the United States.

2. METHODOLOGY

For the radar portion of this study, 38 United States violent tornadic storms from 1993 to 2001 were examined. The "Storm Data" publication was used to determine the time of each violent tornado. The program, "Severe Plot" version 2.0, was obtained from the Storm Prediction Center and was used to determine the location of each violent tornado. The resulting United States map is shown to the left in Figure 1. The tornado tracks for each event are circled.

Figure 1: To the left, the F4 and F5 events are circled on a United States violent tornado map from 1993 to 2001. To the right, the map shows the designated regions of the United States for the radar portion of this study.

For this paper, the United States was divided into five sections shown in the right portion of Figure 1. The divisions were made so that the similarities and differences of the radar characteristics associated with the violent tornado cases could easily be explained in the text. There were ten storms in the Southern Plains, ten storms in the Northern Plains, ten storms in the Southeast, and eight storms in the Northeast.

For this study, we gathered cell and meso data from the algorithm tables and used the .5 degree reflectivity image to analyze radar signatures for each violent tornadic storm from 65 minutes prior to the first violent tornado to ten minutes after the last violent tornado touchdown. We obtained the 1993 to 2001 radar data from the National Climatic Data Center (NCDC). We used the WSR-88D Algorithm Testing and Display System (WATADS) to display the radar data on the Scientific Applications Computer (SAC). As we gathered the data from each violent tornadic storm, we entered each value from the cell and meso tables on a form. We also recorded the violent tornadic storm's radar signatures, cell type and the positioning of the storm relative to other storms around it. After we gathered all the data, we entered the values onto separate spreadsheets for each characteristic. In this way, we created a database with over 15,000 entries. We made graphs showing the average value of all 38 storms at each volume scan during the 65 minutes prior to the first violent tornado to ten minutes after the first violent tornado touchdown. The first volume scan prior to the violent tornado included any data that fell from one to five minutes prior to the violent tornado. The second volume scan included data that fell from six to ten minutes prior to the violent tornado. In this way, we broke each volume scan into five minute intervals. Then, we made graphs of all the data across the United States as well as graphs showing regional data for comparison to other regions.

* Corresponding author address: Chris Broyles, National Weather Service, 1900 English Road, Amarillo, TX 79108

3. RESULTS

The main goal during our research was to make graphs of how different radar characteristics changed during the hour prior to the violent tornado touchdown. The radar signatures that we identified included hooks, pendants, rear flank downdrafts, inflow notches, V-notches, crescent-shaped echoes, and weak echo regions. The main storm characteristics that we considered included cell-based VIL, cell direction of movement, cell top height, meso max rotational velocity, meso gate to gate shear and meso diameter. Other characteristics included cell speed, the value and height of the maximum reflectivity, cell base height, meso strength index, meso rank, meso base height, meso depth, meso low-level rotational velocity, meso maximum shear, meso speed, meso direction of movement, and any tvs or other meso algorithm alerts. The average values for all 38 violent tornadic storms are shown in graphs on the following pages. It is important to note that although the individual storm development varied considerably, the graphs show that there is a distinct process taking place during the hour prior to the violent tornado for the average violent tornadic storm.

3.1 *Cell and Environment Characteristics*

The storm type was determined for each tornadic storm just before the violent tornado touched down. As a result, 35 of the storms were supercells and three were bow echoes. Of the 35 supercells, ten were large supercells, 15 were medium-sized supercells and ten were small supercells. The area of greater than 50 dBZ in large supercells was generally greater than 120 square miles while the area greater than 50 dBZ in small supercells was generally less than 40 square miles. Also to determine size, the storm's dominance and the surrounding cell environment was also taken into account.

Of the 35 supercells, four were rapid developers including one large supercell, one medium-sized supercell and two small supercells. All of the rapidly developing supercells took place in the Great Plains with two in the Southern Plains and two in the Northern Plains. One in the Southern Plains was a large supercell and the other was a medium-sized supercell. The two in the Northern Plains were small supercells.

Of the large supercells, seven of the ten occurred in the Great Plains. Of the medium-sized supercells, 11 of the 15 occurred in the Southern States. Of the small supercells, eight of the ten occurred in the Northern States with four in the Northeast and four in the Northern Plains. Out of the ten small supercells, four were supercell hybrids. Three of the hybrids occurred in the Northeast with one in the Northern Plains. All of the bow echo cases occurred in the East with two in the Northeast and one in the Southeast.

The violent tornadic storm's cell environment was also determined. As a result, 19 of the 38 storms (50 %) were associated with lines. Twelve of the 19 storms occurred within a line of storms with the other seven of the 19 at the absolute north or south end of the line. Six of the 12 storms within a line had a significant clear gap to the south or southwest. Three of the 12 storms within a line had a significant clear gap to the north or northeast. In these cases, the violent tornado occurred

on the storm's south end with no gap to the south or southwest. The other three storms of the 12 within a line were embedded in a solid or nearly solid line. Two of the embedded storms were bow echoes with one being a small supercell hybrid.

The remaining seven storms of the 19 that were associated with lines, occurred at the absolute northern or southern end of the line. Three of the seven storms occurred at the southern end of a line with a clearing in all areas to the south. These were true tail-end charlies. Four of the seven storms occurred at the northern end of a line with a clearing in all areas to the north. In these cases, the violent tornado occurred on the storm's southern end with no gap to the south or southwest. We called these storms hammerhead echoes.

As a result, of all 19 storms associated with lines, nine storms occurred at the southern end of the line with either a clearing in all areas to the south or a gap to the south or southwest within the line. Seven of the 19 storms were hammerhead formations, occurring at the northern end of the line with either a clearing in all areas to the north or a gap to the north or northeast within the line. In these cases, the violent tornado formed on the southern end of the storm.

Of the 19 storms that were not associated with a line, 12 occurred in a storm cluster, six were fairly isolated with one being truly isolated. Of the 12 that occurred within a cluster, seven were on the cluster's south end, four were at the cluster's east end and one was at the cluster's west end. Five of the six fairly isolated storms had other storms away from the storm stretched from the northwest to the northeast. One of the fairly isolated storms had a line to the west. The only truly isolated violent tornadic storm was the Jarrell, Texas large supercell.

Considering regional differences, the three storms that were embedded in a line occurred in the Northern States. Ten of the 16 storms that were associated with a line but not embedded occurred in the Great Plains. Seven of the nine storms that formed at the southern end of a line with all areas clear to the south or a gap to the south or southwest were in the Great Plains. Four of the seven storms that formed at the northern end of a line with all areas clear to the north or a gap to the north or northeast were in the Southeast. All but one of the 12 storms within clusters were in the Northern states and Southern Plains. Four of the six fairly isolated storms were in the Southeast.

For all 38 violent tornadic storms, the average time from cell initiation to the first violent tornado was two hours and ten minutes. The average time from meso initiation to the violent tornado was 20 minutes. The meso here was defined as the actual mesocyclone element that produced the violent tornado, not the first mesocyclone in the storm. Average regional times from initiation to the violent tornado are given in Table 1.

Geographic Region	Time from Cell Initiation	Time from Meso Initiation
Southern Plains	141 min.	14 min.
Northern Plains	102 min.	24 min.
Southeast	170 min.	27 min.
Northeast	117 min.	13 min.

Table 1. The average time from cell and meso initiation to the violent tornado in minutes for each region.

As a result, the storms in the Southeast took the longest to produce the violent tornado from cell and meso initiation. The storms in the Northern Plains took the shortest time from cell initiation and the Northeast storms took the shortest time from meso initiation.

Considering direction of movement, ten of the 11 violent tornadic storms that moved from the south to south southwest were in the Great Plains. In fact, 13 of 20 storms in the Great Plains moved from the south to southwest. Only two Southern Plains storms moved from a different direction being from the north and north northeast. Eight of the ten storms in the Southeast moved from the west southwest or from the west. Seven of the eight Northeast storms moved from a direction anywhere from west southwest to northwest.

As a result, the Great Plains storms generally moved from the south southwest, while the Southeast storms generally moved from the west southwest. The Northeast storms generally moved from the west or from the west northwest.

Considering cell-based VIL, the 38 storm average gradually increased from 60 minutes to 20 minutes prior to the violent tornado. From 20 minutes to five minutes prior to the violent tornado, the rate of increase tripled. In Figure 2 at the top of the page, the Southern Plains cases (typically high CAPE cases) tended to have a strong increase in cell-based VIL at 35 minutes peaking about ten minutes prior to the violent tornado. However, the Northern States and Southeast storms had a cyclic pattern with peaks at 45 minutes and at five minutes prior to the violent tornado with a dip at 30 minutes prior to the violent tornado. The Southern Plains had the highest cell-based VILs

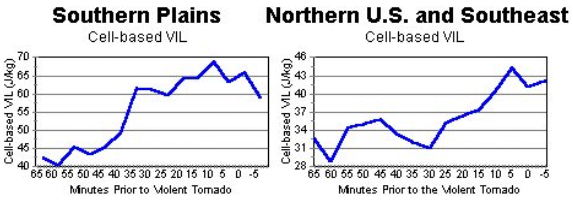

Figure 2. The average cell-based VIL for the ten Southern Plains storms (left) and 28 Northern States and Southeast storms (right).

peaking near 70 J/kg. The Southeast storms were second peaking around 55 J/kg. The Northern States had the lowest peaking from 40 to 45 J/kg.

3.2 *Radar Signatures and Meso Characteristics*

All radar signatures were identified from 65 minutes prior to the violent tornado to ten minutes after the violent tornado using .5 degree reflectivity images. All statistics refer to this time period in the storm's life only. The total number of volume scans evaluated during this period was 509. The table below shows the number of each radar signature found.

Radar Signature	Number	Radar Signature	Number
Pendant	68	Inflow Notch	55
RFD	66	Crescent Shape	33
Hook	59	Weak Echo Region	24
V-Notch	55	Total	360

Table 2. The number of radar signatures found for each type.

As a result, pendant and RFD signatures were the most frequent with hooks, V-notches and inflow notches close behind. When the strongest hook-pendant signature exhibited for each storm was found and the distance from the radar was considered, five of the 38 storms had hooks at greater than 75 miles from the radar. In contrast, five never exhibited a hook during the hour prior to the violent tornado at distances from 39 to 46 miles from the radar. The latter storms might have been difficult to warn for. For the strongest hook-pendant found from each storm, the majority of the hooks occurred from 20 to 52 miles from the radar while the majority of the storms without hooks occurred from 58 to 103 miles from the radar. Twenty-three of the 38 storms (55.3 %) had hooks at some point. Eight of the 23 storms had well-developed hooks. Nine of the 38 (23.7 %) had only pendants while eight (21.1 %) had no hook or pendant observed during the hour prior to the violent tornado.

Each radar signature's strength was taken into account by numbering weak as one, moderate as two and strong as three. Hooks and pendants were given even more detail. The number six was given for well-developed hook, five for hook, four for weak hook, three for hook-like pendant, two for pendant, one for weak pendant and zero was given if there was no hook or pendant. The graph below was made by averaging the strength values for all 38 storms at each volume scan. It shows the hook-pendant occurrence at each time prior to the violent tornado.

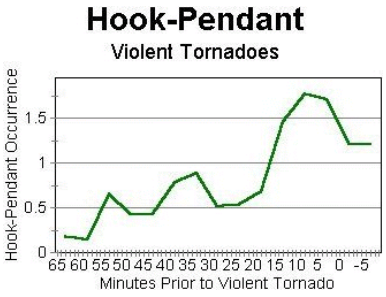

Figure 3. The average hook-pendant occurrence for all 38 violent tornadic storms in the hour prior to the violent tornado.

Notice there were three distinct peaks at 53 minutes, 35 minutes and ten minutes prior to the violent tornado. Troughs occurred at 45 minutes and 25 minutes prior to the tornado. In Figure 4, the average rear flank downdraft (RFD) occurrence for all 38 storms is added onto the hook-pendant graph. For RFD, one was given for weak, two for moderate and three for strong.

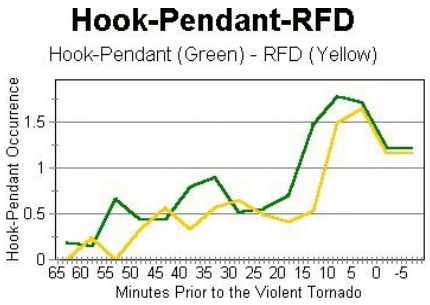

Figure 4. The average RFD occurrence (yellow) is overlaid onto the hook-pendant graph (green) for all 38 storms during the hour prior to the violent tornado.

Notice the RFD signature changes lagged the hook-pendant signature changes by about a volume scan. The three peaks and three troughs in the RFD signature averaged six and a half minutes after the hook-pendant peaks and troughs. The hook-pendant signature more than doubled at about 15 minutes prior to the violent tornado with a three-fold increase in RFD occurrence at ten minutes prior to the violent tornado.

Figure 5 below shows a graph of the average mesocyclone maximum rotational velocity for all 38 storms. Notice the 30 minute up and down cycling period from 53 minutes to 23 minutes prior to the violent tornado. A change occurred at 23 minutes when a strong building period began.

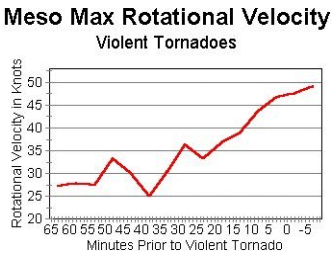

Figure 5. The average meso max rotational velocity (knots) for 38 violent tornadic storms in the hour prior to the violent tornado.

Figure 6 below shows meso gate to gate shear. It is very similar to meso max rotational velocity. Notice the cycling period from 53 to 23 minutes prior to the violent tornado. Notice the strong transition to a building period beginning at 23 minutes. There was a sharp linear increase from 23 minutes continuing until after the violent tornado touched down.

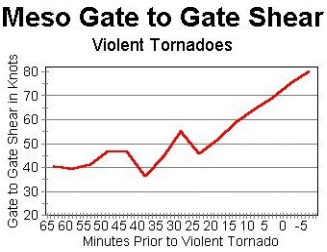

Figure 6. The average meso gate to gate shear (knots) for 38 violent tornadic storms in the hour prior to the violent tornado.

Figure 7 shows meso gate to gate shear overlaid onto the hook-pendant occurrence. Notice the gate to gate shear peaks at 46 minutes and 28 minutes prior to the violent tornado. These peaks coincide with the troughs for hook-pendant occurrence.

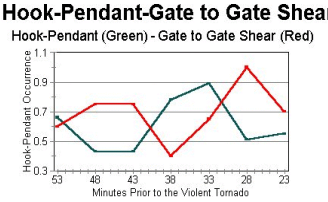

Figure 7. Gate to gate shear in knots (red) overlaid on hook-pendant occurrence (green) from 53 to 23 minutes prior to the violent tornado.

In figure 8 below, the RFD graph is overlaid onto the meso gate to gate shear graph. Notice that during the 30 minute cycling period from 53 minutes to 23 minutes prior to the violent tornado, there is a similarity between RFD and meso gate to gate shear. This similarity is also true for RFD and meso max rotational velocity. Notice during the rapid building period, the meso gate to gate shear does not react to the strong surgence of the RFD with only a very slight reaction by meso max rotational velocity (Figure 5). The mesocyclone during the rapid building period is very strong and stable. The lack of fluctuation and the linear increase can partially be explained by an idea taken from (Brooks et al. 1993) which states that mid-level shear is important to sustaining stable long-lived mesocyclones especially at low-levels. This idea is supported by the synoptic portion of our study which showed that 34 of the 38 violent tornado events occurred either just ahead of or in the core of the 700 mb or 500 mb jet. With the approach of the mid-level jet, the 3 to 7 kilometer shear would steadily increase. In the 34 cases, this approach of the mid-level jet coincides with the building period of the mesocyclone during the 23 minutes prior to the violent tornado. It is possible that increased mid-level shear from the approach of the mid-level jet explains why the strong stable mesocyclone strengthens in such a linear fashion during the rapid building period.

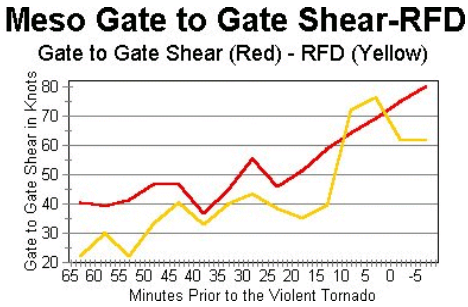

Figure 8. The average RFD occurrence (yellow) is overlaid onto the meso gate to gate shear graph in knots (red) for all 38 storms during the hour prior to the violent tornado.

The graphs in Figure 3 through Figure 8 present a dilemma for the radar operator. Take a scenario for instance. If a tornadic storm followed the averages for the 38 storms, the hook or pendant signature would become apparent at 53 minutes prior to the violent tornado. The radar operator would see the meso max rotational velocity and gate to gate shear increase at 48 minutes prior to the violent tornado. With the radar signatures and meso velocities coming up, the radar operator issues a tornado warning valid for 30 minutes. During the tornado warning, the hook echo signature peaks strongly at 35 minutes prior to the violent tornado followed at 30 minutes by an increase in the RFD, meso max rotational velocities, and meso gate to gate shear. From 33 minutes to 23 minutes prior to the violent tornado, the hook decreases or disappears which is followed by a weakening RFD. From 28 minutes to 23 minutes, the meso max rotational velocity and meso gate to gate shear come down. At 23 minutes prior to the violent tornado, only five minutes are left before the tornado warning expires. The radar operator must make a decision to extend the tornado warning or downgrade to a severe thunderstorm warning. In this scenario based on our 38 cases, with the radar signatures decreasing, cell top height coming down (see Figure 11) and meso velocities decreasing, the radar operator decides to downgrade to a severe thunderstorm warning. Now the radar is lighting up and the radar operator needs to devote his attention to other storms. Little does he know, the violent tornadic storm is about to rapidly intensify. He or she will need to react quickly and upgrade once again to a tornado warning as the rapid building period of the mesocyclone occurs prior to the violent tornado.

In figure 9 at the top of the next page, meso diameter is shown with the RFD graph overlaid. Notice the strong relationship between meso diameter and RFD. The three peaks occur at about the same time with the meso diameter peaking a few minutes before the RFD at each peak. On a larger time scale, the difference is that the meso diameter decreases and the RFD increases during the hour prior to the violent tornado. On a smaller time scale, as the meso diameter increases, the RFD increases. The meso velocities also increase reacting to an increase of the RFD (only during the cycling period). As the meso diameter decreases, the RFD decreases. And when the RFD decreases, the meso velocities go down (only during the cycling period). What may be happening during the cycling period is that when the meso size increases, it has more influence on the neighboring environment and pulls the RFD around deepening the meso resulting in higher meso velocities. When the meso size decreases, it loses influence and the RFD weakens. The meso fills and the meso velocities decrease ending the cycle.

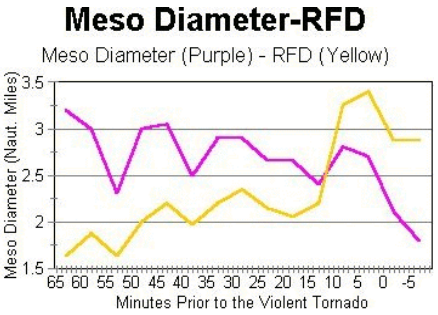

Figure 9. RFD (yellow) overlaid on meso diameter in nautical miles (purple) for all 38 storms in the hour prior to the violent tornado.

When the cycling period ends at 23 minutes, a significant reversal occurs. In Figure 10, meso gate to gate shear is overlaid onto the meso diameter graph. Notice the sharp reversal at 23 minutes. At this time, the strong and stable mesocyclone begins to strengthen linearly and the meso diameter begins to shrink. This shrinking and strengthening stage continues for ten minutes until the strong surgence of the RFD beginning at 13 minutes prior to the violent tornado. The meso velocities in the large

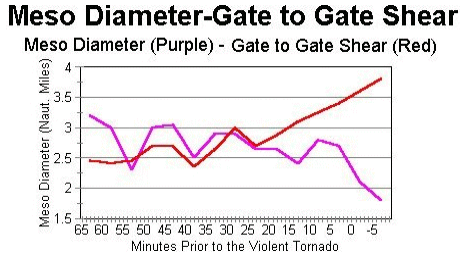

Figure 10. Meso gate to gate shear in knots (red) overlaid onto the meso diameter graph in nautical miles (purple) for all 38 storms in the hour prior to the violent tornado.

stable mesocyclone do not react to the surgence of the RFD but the meso diameter does widen or stretch. The shrinking stage is temporarily interrupted. When the RFD begins to weaken at three minutes prior to the violent tornado, a strong snap back occurs. The strong and large mesocyclone then snaps back into the rapidly shrinking state. The meso diameter shrinks quickly by 25 % as the violent tornado touches down.

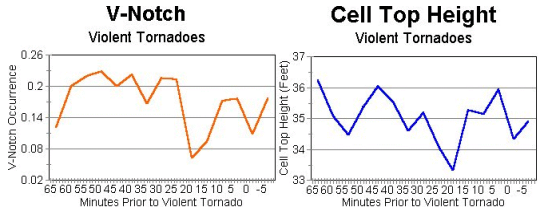

Figure 11. V-notch (left) and cell top height in feet (right) for 38 violent tornadic storms in the hour prior to the violent tornado.

At the left in Figure 11, a graph for V-notch is shown for all 38 violent tornadic storms. Notice the V-notch occurrence decreases in the hour prior to the violent tornado. There is a sharp decrease at 18 minutes prior to the violent tornado. This is the result of a collapsing storm top which is shown to the right in Figure 11. Notice the cell top height drops sharply with a trough at 18 minutes prior to the violent tornado matching the V-notch trough. Rapid hook formation occurs just after the storm top collapse. Then, the storm top collapse causes a sudden and very strong surgence of the RFD. This all happens in the first half of the rapid building period of the mesocyclone.

At the left in Figure 12 at the top of the page, a graph for inflow notch is shown for all 38 violent tornadic storms. Notice the two sharp peaks at 43 minutes and 23 minutes for inflow notch coincide with the troughs for hook-pendant occurrence. This shows that as the hook or pendant weakens, the inflow notch occurrence increases. These peaks occur just after peaks in the RFD occurrence and meso velocities. The middle graph in Figure 12 shows weak echo region. Notice the two peaks at 48 minutes and at 23 minutes. Like inflow notch, the peaks in the weak echo region coincide with the troughs in the hook-pendant signatures. The weak echo region appears during the times of strong inflow and near or just after the peak

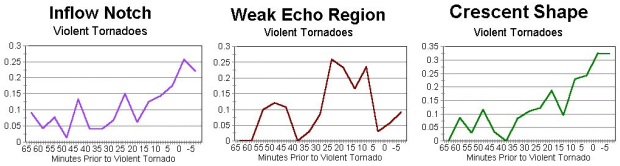

Figure 12. Inflow notch (left), weak echo region (middle) and crescent shape (right) for 38 violent tornadic storms during the hour prior to the violent tornado.

in meso velocities. At the right in Figure 12, a graph for crescent shape is shown. Notice that the crescent-shaped appearance of the echo steadily increases during the 40 minutes prior to the violent tornado.

4. SUMMARY

The radar characteristics for violent tornadic storms contain a broad spectrum. Most of the violent tornadic storms were supercells with only a few bow echoes. The supercells varied in size from miniature-sized to large dominant storms. And the storms formed in a variety of storm cell environments associated with lines, clusters, or being fairly isolated. When radar signatures were considered, pendants and rear flank downdraft signatures were the most frequent.

To summarize from our 38 storm average, there is a cycling period from 53 minutes to 23 minutes prior to the violent tornado. From 23 minutes until the violent tornado, there is a strong mesocyclone building period. During the cycling period, two distinct cycles occur. Each cycle begins when the meso diameter rapidly shrinks. At this time, the mesocyclone fills causing the meso rotational velocities to weaken. As the meso shrinks, the hook or pendant strengthens. The hook or pendant peaks when the meso is small and close to the precipitation shaft. The cell top collapses a bit during this period. Three to five minutes later, the meso diameter increases causing the hook to decrease or disappear. The larger mesocyclone then pulls the RFD around. This deepens the mesocyclone and the meso velocities go up. Near or just after this time, inflow notch and weak echo region signatures appear relating to strong inflow. As the RFD weakens, inflow takes over, the meso velocities go down and the meso shrinks ending the cycle. At 23 minutes prior to the violent tornado, the hook or pendant, RFD and meso velocities are all decreasing. As a result, the cell top collapses causing the V-notch to disappear. However, during this time, the cycling period ends and the strong stable mesocyclone begins to rapidly build. The meso velocities begin to linearly increase possibly resulting from a steady increase in mid-level shear. As the meso velocities go up, the meso diameter steadily shrinks causing the hook to rapidly develop beginning at 18 minutes. The storm top collapse causes a strong surge of the RFD beginning at 13 minutes prior to the violent tornado. This causes the meso to increase in diameter, temporarily interrupting the shrinking stage of the meso. When the RFD begins to weaken at three minutes prior to the violent tornado, a strong snap back occurs. The strong and large mesocyclone then snaps back into the rapidly shrinking state. The meso diameter shrinks quickly by 25 % as the violent tornado is born. For a color webpage of this study, go to http://www.srh.noaa.gov/ama/html/Violenttornadoes.html.

To conclude, many ideas have been presented for violent tornadic supercells. It is hoped that the reader came away with an increased understanding of violent tornadic storms. Hopefully, this paper will better help prepare the radar operator for the next violent tornadic supercell that comes their way.

5. REFERENCES

Brooks, H., C. Doswell, and R. Wilhelmson, The Role of Midtropospheric Winds in the Evolution and Maintenance of Low-level Mesocyclones. Mon. Wea. Rev., **122**, 126-136.

Burgess, D.W. and L.R. Lemon, 1990: Severe Thunderstorm detection by radar in Radar in Meteorology (D. Atlas, ed.), Amer. Meteor. Soc., Boston, 619-647 pp.

Burgess, D.W., M. Magsig, J. Wurman, D. Dowell, and Y. Richardson, 2001: Radar observations of the 3 May 1999 Oklahoma City tornado. Submitted to Wea. and Forecasting.

Burgess, D.W. and M.A. Magsig, 1998: Recent observations of tornado development at near range to WSR-88D radars. Preprints, 19th Conf. on Sev. Local Storms, Sep 14-18, Amer. Met. Soc., Minn., MN, 756-759.

Carpenter, E., A. Gerard, and Agre, E.: An Analysis of NSSL WDSS Circulation Parameters during 1999-2000 Tornado Events in the NWS Jackson, Mississippi, County Warning Area. Preprints, 20th Conf on Sev. Local Storms, Sep 11-15, Amer. Met. Soc., Orlando, FL 368-370.

Markowski, P., E. Rasmussen, and J. Straka, 2000: Surface Thermodynamic Characteristics of RFDs as Measured by a Mobil Mesonet, Preprints, 20th Conf on Sev. Local Storms, Sep 11-15, Amer. Meteor. Soc., Orlando, FL 251-254.

Stumpf, G. J., Ed., 1999: NWS Tornado Warning Guidance. http://www.osf.noaa.gov/otb/PAPERS/twg99/index.htm

For Additional References See Papers JP1.4 and JP1.5 and the webpage